Biochimica et Biophysica Acta 1838 (2014) 1082–1087

Contents lists available at ScienceDirect

Biochimica et Biophysica Acta

journal homepage: www.elsevier.com/locate/bbamem

Mechanistic insights from functional characterization of an unnatural His37 mutant of the influenza A/M2 protein ☆

Alexei L. Polishchuk [a,1], Lidia Cristian [a,2], Lawrence H. Pinto [b], James D. Lear [a,3], William F. DeGrado [a,*,4]

[a] Department of Biochemistry and Biophysics, The Robert Wood Johnson Foundation, University of Pennsylvania, Perelman School of Medicine, Philadelphia, PA 19104, USA
[b] Department of Neurobiology and Physiology, Northwestern University, Evanston, IL 60208, USA

ARTICLE INFO

Article history:
Received 31 May 2013
Received in revised form 2 October 2013
Accepted 12 November 2013
Available online 22 November 2013

Keywords:
Influenza
M2
Proton
Transport
His37
pK_a

ABSTRACT

The influenza A/M2 protein is a homotetrameric single-pass integral membrane protein encoded by the influenza A viral genome. Its transmembrane domain represents both a crucial drug target and a minimalistic model system for transmembrane proton transport and charge stabilization. Recent structural and functional studies of M2 have suggested that the proton transport mechanism involves sequential extraviral protonation and intraviral deprotonation of a highly conserved His37 side chain by the transported proton, consistent with a pH-activated proton shuttle mechanism. Multiple tautomeric forms of His can be formed, and it is not known whether they contribute to the mechanism of proton shuttling. Here we present the thermodynamic and functional characterization of an unnatural amino acid mutant at His37, where the imidazole side chain is substituted with a 4-thiazolyl group that is unable to undergo tautomerization and has a significantly lower solution pK_a. The mutant construct has a similar stability to the wild-type protein at pH 8 in bilayers and is virtually inactive at external pH 7.4 in a semiquantitative liposome flux assay as expected from its lower sidechain pK_a. However when the external buffer pH is lowered to 4.9 and 2.4, the mutant shows increasing amantadine sensitive flux of a similar magnitude to that of the wild type construct at pH 7.4 and 4.9 respectively. These findings are in line with mechanistic hypotheses suggesting that proton flux through M2 is mediated by proton exchange from adjacent water molecules with the His37 sidechain, and that tautomerization is not required for proton translocation. This article is part of a Special Issue entitled: Viral Membrane Proteins — Channels for Cellular Networking.

1. Introduction

The influenza A/M2 protein (M2) is a multi-modular 97 residue integral membrane protein encoded by the viral genome that forms a parallel homotetramer in the viral envelope and is required for multiple functions in viral replication [1]. Its transmembrane domain mediates passive, N-terminal acid activated, pH-regulated proton transport that is inhibited by the antiviral agents amantadine and rimantadine in increasingly rare sensitive circulating influenza strains [2,3]. M2 is thus of interest not only as a clinically important drug target but also as a model system of structurally minimalistic [4], highly regulated transmembrane proton transport with a high degree of charge stabilization in the pore [5].

The proton transport properties of M2 have been under extensive study for several decades, and our understanding of its mechanism of conduction and charge stabilization has been recently accelerated with the advent of high-resolution TM domain structures and improved solid state NMR techniques [1]. Mutagenesis experiments have shown that two pore-lining residues in the M2 transmembrane domain (M2TM), His37 and Trp41 are required for proton selectivity and N-terminal acid activation, respectively [6,7]. Early mechanistic hypotheses suggested that M2 may function as an electrostatic gate, where sequential protonation of His37 residues opens the pore for proton conduction across water wires in a Grotthuss style mechanism [8]; however, this mechanism is inconsistent with functional studies showing that M2 proton transport saturates at a much lower rate than the diffusion-limited process that this mechanism would predict [9].

Abbreviations: M2TM, M2 transmembrane domain; POPC, 1-Palmitoyl-2-oleoyl-*sn*-glycero-3-phosphocholine; POPG, 1-Palmitoyl-2-oleoyl-*sn*-glycero-3-phospho-(1′-*rac*-glycerol) (sodium salt); DLPC, 1,2-Dilauroyl-*sn*-glycero-3-phosphocholine; nOG, n-Octyl-β-D-glucoside; HPTS, 8-Hydroxypyrene-1,3,6-trisulfonic acid; DPX, *p*-Xylene-bis-pyridinium bromide; TCEP, *Tris*(2-carboxyethyl)phosphine

☆ This article is part of a Special Issue entitled: Viral Membrane Proteins — Channels for Cellular Networking.

* Corresponding author at: 555 Mission Bay Boulevard South, San Francisco, CA 94158-9001, USA. Tel.: +1 415 502 0272; fax: +1 415 502 4690.
E-mail address: William.DeGrado@ucsf.edu (W.F. DeGrado).
[1] Present address: Department of Radiation Oncology, University of California, San Francisco, CA 94115, USA.
[2] Present address: Influmedix Inc., Radnor, PA 19087, USA.
[3] Present address: Higher Ground Outfitters, Magdalena, NM 87825, USA.
[4] Present address: Department of Pharmaceutical Chemistry, University of California, San Francisco, CA 94158, USA.

0005-2736/$ – see front matter © 2013 Elsevier B.V. All rights reserved.
http://dx.doi.org/10.1016/j.bbamem.2013.11.011

Another hypothesis derived from functional characterization of sequential Cys mutants of the transmembrane domain suggested that M2 conducts protons as a histidine shuttle [10], where the His37 imidazole groups are protonated from water molecules within the extraviral aspect of the pore and deposit their protons onto water molecules in the intraviral aspect of the pore. This mechanism suggests that the conduction speed limit is likely determined by the pK_a of the His37 residue, and specifically the deprotonation step which is predicted to be much slower than the protonation step [11]. This mechanism is consistent with the saturating behavior of proton transport seen in functional studies [9,12].

Recently determined high resolution structures of the M2 transmembrane domain at a variety of pH values in micelles [5,13–15] suggested that the pore populates a pH dependent conformational ensemble [16] with the extraviral Val27 gate becoming progressively more closed at low external pH, restricting extraviral proton access to His37, and the intraviral Trp41 gate becoming progressively more open, allowing greater access to His37 from the intraviral side to suggest a transporter-like conduction cycle where conformational changes alternately expose the cargo binding site to either side of the membrane. A fluorescence quenching study with the full length protein reconstituted in bilayers [12] supported the notion of a pH-dependent conformational equilibrium at the transmembrane domain, and good fits to externally acquired functional data could be achieved with an activated, cyclic kinetic mechanism involving rapid conformational transitions between two structural variants with the overall rate-limiting step being His37 residue deprotonation on the intraviral aspect of the pore [12]. More recent NMR studies imply a role for backbone conformational transitions in facilitating proton conduction, but there is no experimental evidence that these steps are rate-limiting [17,18].

Pending more detailed experimental investigation of the requirement for backbone conformational changes in the M2 conduction mechanism, the focus remains on the interaction of the permeant proton with the His37 tetrad as the critical process in proton transport, with the proton release step postulated to be rate-limiting. Several hypotheses exist as to the sidechain-level mechanistic transitions mediating this interaction.

Prior to the existence of atomic-resolution M2 structures, Pinto and colleagues used mutagenesis to derive a structural model suggesting a conduction cycle of His37 protonation and deprotonation with intermediate steps of sidechain imidazole ring-flipping or tautomerization [10]. This hypothesis was supported by a high-resolution crystal structure of the M2TM tetramer in detergent micelles obtained at intermediate pH, where the tetrad of His37 sidechains (the "His box") is oriented parallel to the transmembrane axis and surrounded by a highly ordered hydrogen-bonded water network presumed to stabilize the permeant proton and the protonated His-box intermediates [5]. The "His box" ring-flip mechanism was also supported by recent solid state NMR characterization of M2 reconstituted in native-like membranes, where His37 ring flip, protonation, and deprotonation were shown to take place on roughly the same timescale of 10^5 s^{-1} and were significantly inhibited by the addition of amantadine [17]. No evidence for rapid inter-tautomer exchange at the His37 imidazoles as initially postulated by Pinto et al. [10] was seen in other NMR experiments conducted by this group [19]. Of note, the protonation, ring flip and deprotonation timescales described in Ref. [17] are 1–2 orders of magnitude faster than M2 conduction rates calculated in vesicle assays performed by multiple groups, [4,20–22] suggesting that the protein either does not attain its speed limit in the conditions employed in vesicle assays or that other steps may also limit its conduction rate.

A second hypothesis for proton permeation suggests that the His37 tetrad partitions into a dimer of dimers stabilized by low-barrier intersidechain hydrogen bonds [23] which forms the resting state in the transport mechanism. This dimer is disrupted by the permeant proton, and the protonated imidazolium intermediate is stabilized by a nearby Trp41 sidechain. This mechanism is supported by a M2 tetramer structure obtained through solid-state NMR spectroscopy in bilayers and by ab initio modeling [18,24], and does not rule out imidazole ring flipping as part of proton transport. While NMR experiments by other investigators did not observe this low-barrier hydrogen bonded imidazolium dimer [25], more recent work suggests that both mechanisms may play a role in M2 proton conduction [26].

Here we extend our understanding of the M2 proton transport mechanism with a functional characterization of an unnatural amino acid mutant of M2 at position 37, where the imidazole heterocyclic ring is replaced with a 4-thiazole group that has a significantly lower solution pK_a (2.55 vs ~6.5) and is incapable of tautomerization (Fig. 1). Previously published chemical rescue experiments by Pinto et al. indicated that M2 His37Gly regained function with added buffer components that sterically and electronically resembled imidazole [27]. We find that the thiazole-substituted M2TM construct shows similar stability to wild-type peptide in pH 8 in bilayers, and that a longer construct involving the TM domain and the C-terminal amphiphilic helix is largely inactive in a liposome flux assay at pH 7.4 as predicted by the low pK_a of the thiazole side chain. The mutant construct shows a pH-dependent pattern of increasing amantadine sensitive proton flux at pH 4.9 and 2.4 that is similar in magnitude to flux through the wild type construct at pH 7.4 and 4.9 respectively, suggesting that proton conduction through M2 is highly tuned to the pK_a at the His37 side chain, and, as indicated in recent ssNMR experiments, does not necessarily require His37 side chain tautomerization [19].

2. Materials and methods

2.1. Peptide preparation and purification

Peptides (M2 constructs of length 19–46 and 19–62 using the A/Udorn/72 sequence with the C50S mutation; 19-NH2-CNDSSDPLV VAASIIGILHLILWILDRL-(-$CONH_2$-46)-FFKSIYRFFEHGLKRG-$CONH_2$-62) were synthesized by Fmoc solid-phase chemistry as C-terminal carboxamides, and were N-terminally amidated to protect the Cys 19 sidechain. Peptides were synthesized on an Applied Biosystems 433A synthesizer, or, for the longer constructs, manually using a CEM Mars microwave heated reactor, with frequent reaction monitoring. Fmoc-protected L-4-thiazolylalanine was purchased from Synthetech (Albany, OR) and used without further purification in place of Fmoc-His(Trt)-OH at position 37 in the mutant peptide. Peptides were cleaved from the resin and purified using RP-HPLC according to previously described procedures [4,28].

2.2. Thermodynamic stability studies of M2(19–46) constructs using thiol–disulfide equilibria

Thermodynamic studies of tetramer stability of the M2(19–46) WT and mutant constructs in DLPC bilayers were performed according to a previously described protocol [28].

Small unilamellar vesicles were prepared by codissolving M2TM 19–46/trifluoroethanol stock solutions with the appropriate amount of DLPC (Avanti Polar Lipids) from a stock solution in ethanol. The solvent was evaporated under a stream of nitrogen, and the protein/phospholipid film was kept overnight under high vacuum to remove all traces of solvent. The dry peptide/phospholipid films obtained were then hydrated in buffer (0.1 M Tris·HCl/0.2 M KCl/1 mM EDTA, pH 8.6), vortexed, and sonicated to clarity by using a bath sonicator (Laboratory Supplies, Hicksville, NY). The concentration of peptide (20 μM) was kept constant while varying the phospholipid concentration to attain the desired peptide/phospholipid mole ratios (typically between 1:100 and 1:1500).

Reversible disulfide formation was initiated by adding oxidized glutathione (GSSG) and reduced glutathione (GSH) at varying ratios to the samples as previously described [29]. The time required for the equilibration of the samples was determined by analyzing aliquots of

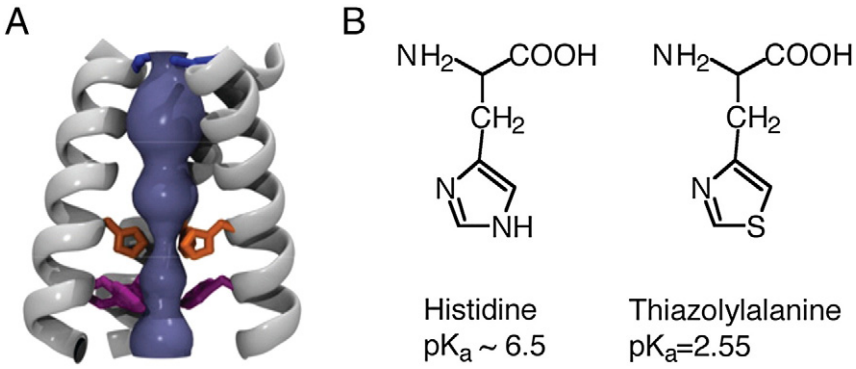

Fig. 1. Nature of His37 unnatural amino acid substituent. A. Three-dimensional representation of the M2TM domain with His37 sidechains highlighted in orange and Trp41 sidechains highlighted in purple, (PDB ID: 3LBW). B. Chemical structure and pK_a values of histidine and 4-thiazolylalanine.

the reaction mixture at different times by analytical reverse-phase HPLC. To ensure equilibration between the vesicles, the samples were freeze-thawed every hour during the equilibration, using a dry ice–acetone bath for freezing and a bath sonicator during thawing, followed by sonication to clarity. After equilibration, the reactions were quenched by lowering the pH.

The components of the equilibrium mixtures were analyzed by reverse-phase HPLC. They typically consisted of a mixture of three species corresponding to the thiol-free peptide, mixed disulfide of peptide with GSH, and disulfide-bonded peptide. These species were identified by using matrix-assisted laser desorption ionization-time of flight MS. A small amount of the reaction mixture was used to determine the total free thiol content at the end of the reaction by using Ellman's reagent, 5,5′-dithiobis(2-nitrobenzoic acid). The amount of covalent dimer was calculated from the integrated HPLC peak areas of the present species in the chromatograms by using the software supplied with the HPLC.

The data obtained from thiol–disulfide exchange measurements were fit to a fully cooperative monomer–tetramer equilibrium as previously described [28] where the fully reduced tetrameric species could subsequently be partially (one disulfide bond) and then fully oxidized (two disulfide bonds) at equilibrium. A baseline correction was employed as previously described [28].

Raw data in this assay were reproducible within 5% and the curve fitting pK_{tet} was reproducible to within one unit (one order of magnitude) in multiple fit trials.

2.3. Liposome flux assay

2.3.1. Determination of proton flux through M2 constructs incorporated into liposomes using a pH-sensitive fluorescent dye

Functional studies of the WT M2(19–62) constructs and the thiazolyl histidine mutant were performed largely according to the protocol described in Ref. [4].

2.3.1.1. Sample preparation. Lipid films consisting of 4:1:2 POPC:POPG:cholesterol (25 μmol total) were made by nitrogen or argon gas stream evaporation of mixed freshly opened chloroform stocks of the phospholipids (POPC and POPG, 25 mg/mL, Avanti Polar Lipids, Alabaster, AL) and a fresh chloroform stock of powder cholesterol (25 mg/mL, Sigma Aldrich, St. Louis, MO). The resulting lipid films were dried on a lyophilizer for at least two hours. Only Teflon, metal and glass components were used to handle the chloroform stocks to prevent leaching of plasticizers from plastic components.

Peptide concentration was quantified by using absorbance at 280 nm in an ethanol stock, with ε_{280} for M2(19–62) of 6990 M^{-1} cm^{-1}. Lyophilized peptides (as trifluoroacetate salts from HPLC purification) were dissolved in ethanol and the fragment concentration was determined. Stocks were maintained on dry ice or at −80 °C until use. Peptide in ethanol in an amount of 25 nmol monomer was added to a lipid film (target 1:1000 monomer:lipid ratio); additional ethanol was added to a total volume of approximately 300 μL. For control liposomes, only ethanol was added. The mixture was vortexed to dissolve the dried lipid, then immediately dried under an argon stream.

The resulting film was immediately hydrated with 990 μL "K" buffer (50 mM K_2SO_4, 15 mM K_xPO_4 pH ~7.5) by vortexing for 2 min. The mixture was frozen on dry ice and thawed. 10 μL of 100 mM of the fluorescent pH indicator hydroxypyrene trisulfonic acid trisodium salt (HPTS, pyranine from Invitrogen) was then added, and the mixture vortexed. Unilamellar liposomes were formed by 10 freeze–thaw cycles (dry ice/ethanol and 37 °C water bath) and sized by repeated passage through 100 nm polycarbonate filter membranes (Whatman, Piscataway, NJ) in a mini-extruder (Avestin, Ottawa, Canada). Liposomes were then dialyzed overnight in a 10 K MWCO Pierce Slide-A-Lyzer cassette against 1.8 L of "K" buffer pH 7.40 (adjusted with H_3PO_4 or KOH) with 5 g Amberlite XAD-4 resin (Supelco, Bellefonte, PA) added to bind unincorporated dye. Dialyses were performed at 4 °C. Liposomes were stored at 4 °C for up to a week following the completion of dialysis.

2.3.1.2. Proton flux assay. Experiments were performed using an Aviv ATF-105 spectrofluorometer (Aviv Biomedical, Lakewood, NJ) in a 1 × 1 cm Hellma (Plainview, NY) QS fluorescence cell, thermostated at 18 °C. The ratiometric pH indicator HPTS (pyranine, pK_a ~ 7.22) was used to determine intraliposomal pH. The ratio of fluorescent signal of the deprotonated form (excitation 460 nm, emission 515 nm, "F^-") to the pH-independent isosbestic point (excitation 417 nm, emission 515 nm, "F_{iso}") as a function of pH was used to calibrate the assay and was largely independent of the presence of liposomes. For all samples measured with amantadine, liposomes were pre-mixed with 100× aqueous amantadine HCl (Sigma Aldrich, St. Louis, MO) in a 100:1 v/v ratio and allowed to interact for three hours so as to achieve equilibrium binding.

2.3.1.3. Assay buffers. 2.5 mL of assay buffer (50 mM Na_2SO_4, 15 mM Na_xPO_4 pH 7.4, 4.9, or 2.4 adjusted with H_3PO_4 or NaOH, "Na buffer") was added to the fluorescence cuvette. To the assay "Na" buffer was added 37.5 μL of 1 M *p*-xylene bis-pyridinium bromide (DPX; Invitrogen, Carlsbad, CA), a membrane impermeable quencher of pyranine fluorescence to restrict measured signal to intraliposomal HPTS. To trigger proton flux, 3.5 μL of 18 μM valinomycin acting as potassium ionophore to trigger a transmembrane potential (Fluka/Sigma Aldrich, St. Louis, MO) was added from an ethanol stock. Valinomycin was added at a predicted ~1:1 valinomycin:functional tetramer ratio. Where amantadine inhibition was tested, 25 μL of 100× aqueous amantadine hydrochloride was also added to the assay buffer.

2.3.1.4. Data collection. Prior to data collection, the assay buffer (with DPX, valinomycin and drug as indicated) was allowed to equilibrate at 18 °C for 5 min in the fluorometer cell holder. Liposomes (~20 μL) were injected into the cuvette containing assay buffer from a 1 mL Hamilton (Reno, NV) glass syringe fitted with a repeat-dispensing system. Injections (at t = 0 s) were performed through an adapter in the fluorometer cell holder cover that enabled immediate data acquisition following injection. The sample in the cuvette was vigorously stirred during the experiment. From t = 0 s, kinetic data monitoring the deprotonated form of HPTS (F^-, ex 460 nm, em 515 nm, bandwidths 2 nm) were collected for approximately 50 s at one second intervals. The first three seconds following injection were omitted from analysis to allow for full mixing of the sample. At t = ~90 s, kinetic data monitoring the pH-independent isosbestic point of HPTS (F_{iso}, ex 417 nm, em 515 nm, bandwidths 2 nm) were collected for approximately 20 s at one second intervals. An excitation wavelength scan (ex 480–380 nm, em 515 nm, bandwidths 2 nm) was performed at the conclusion of each experiment for secondary confirmation of the result. Experiments on each condition were performed in triplicate.

2.3.1.5. Liposome Flux Assay Data Analysis. The measured isosbestic kinetic signal (F_{iso}, ex 417 nm, em 515 nm) was averaged to a single value when experiments were performed at a bathing buffer pH_{out} of 7.4, and each data point from the deprotonated HPTS signal kinetic (F^-, ex 460 nm, em 515 nm) was divided by the isosbestic signal average to obtain a signal ratio (deprotonated:isosbestic) as a function of time.

During experiments done at pH_{out} 4.9 and 2.4, noticeable decreases in the isosbestic signal of HPTS, F_{iso} (ex 417 nm, em 515 nm) were observed compared to runs performed at pH_{out} 7.4, which suggests that some dye may be leaking out of the liposomes at low pH conditions, or that the isosbestic wavelength may not be set with sufficiently high precision. To correct for this effect, the F_{iso} signal for a given set of liposomes determined in low pH experiments (e.g. control, WT, ThiazolylAla) was linearly normalized to its value determined from experiments performed at pH_{out} 7.4, since a similar volume of liposomes was added for each run.

More specifically, the time-averaged F_{iso} signals (obtained at ~90–120 s following experiment start) from triplicate runs under each condition were further averaged amongst themselves, and ratios of these values obtained at pH 4.9 vs. pH 7.4 and pH 2.4 vs. pH 7.4 were calculated. Recording of the F_{iso} signal began approximately 90 (t = 90–120 s) seconds following the start of each run, and the F^- signal was recorded for the first ~45 s (t = 0–45 s) of each run. The time-averaged F_{iso} signal for each low pH run was extrapolated to earlier timepoints with the following operation:

$$F_{iso}(t, pH(X)) = F_{iso(t=90\ \text{to}\ 120, pH(X))}\left[1 + \left(\frac{AvgF_{iso}(pH\,7.4)}{AvgF_{iso}(pH(X))} - 1\right)\left(1 - \frac{t}{90}\right)\right].$$

The F^-/F_{iso} ratios at each time point were then averaged between the three independent experiments run for each condition, and the averaged ratios were used to calculate the intraliposomal pH according to a previously determined HPTS pH calibration curve. Plots of these ratios (F^-/F_{iso}) vs. time following the above corrections are shown in supplementary Figs. S1–S3 with error bars reflecting the associated standard deviations from triplicate runs. Excellent reproducibility was observed in these assays as shown.

Intraliposomal pH ($-\log[H^+_{free}]$) vs. time was converted to total intraliposomal [H^+] vs time (including H^+ bound to buffer) by using an estimate of the internal buffering capacity [30] assuming an intraliposomal [phosphate] of 15 mM, and negligible contribution to buffering capacity by the dye given its much lower concentration.

Total intraliposomal [H^+] vs. time was converted to the total intraliposomal proton count vs. time through multiplication by N_A and intraliposomal volume estimated from dynamic light scattering measurements (described below) assuming no phospholipid loss during preparation and a single phospholipid surface area of 6.3×10^{-19} m^2. Experiments with tracer amounts of radiolabeled lipid show that signal loss during typical preparations is <10%.

The initial number of total protons at t = 3 s was subtracted from successive measurements, and the result was divided by the number of peptide tetramers delivered per experiment, as estimated by integration of the 280 nm protein peak from chromatography of proteoliposome samples on an analytical RP-HPLC column (see below).

Results for protein-free control liposomes were adjusted for differences in surface area with fragment-containing liposomes, and were normalized for the degree of protein reconstitution observed for the fragment in each panel (i.e. the difference in total H^+ vs. time traces for the control liposomes was divided by the same number of peptide tetramers as determined for the corresponding protein-containing sample shown in each panel).

2.3.2. Estimate of liposome peptide reconstitution

Liposome samples were mixed in a 2:1 ratio with a lysis buffer containing 150 mM nOG and 150 mM Tris pH 8. 100 mM TCEP HCl (~6% v/v) was added to all samples. The mixture was then injected onto an analytical C4 RP-HPLC column and eluted with a linear gradient of 2:1 isopropanol:acetonitrile with 0.1% TFA and water with 0.1% TFA. Peptide incorporation was quantified using a standard curve (four calibration points fitted with linear regression, $R^2 = 0.95$) using extinction coefficients of 6990 M^{-1} cm^{-1} at 280 nm wavelength for both WT and thiazole constructs. In subsequent calculations, random peptide orientation within the bilayer was assumed and the calculated tetramer population was divided by two to reflect this.

2.3.3. Determination of liposome volume and surface area

Liposome radii were determined using a Wyatt (Santa Barbara, CA) DynaPro dynamic light scattering instrument at 25 °C. Liposomes were diluted ~1:1000–1:10,000 into pre-filtered "K" buffer. Measurements were performed in triplicate for each sample, and the radius distribution peak maxima were averaged. Standard deviations of these measurements were within 5%.

Volumes and surface areas were determined based on the averaged measured radius. The software of the instrument was set for analysis based on a Rayleigh sphere model, and the solvent model was set to phosphate buffered saline.

3. Results

3.1. M2(19–46) His37(4-thiazolyl)Ala mutant shows similar tetramer stability to wild type peptide in bilayers

We first set out to determine whether substitution of the sterically similar yet electronically distinct 4-thiazole heterocycle for the imidazole at position 37 significantly perturbed the thermodynamic stability of the M2TM tetramer. Thermodynamic studies of tetramer stability of M2(19–46) WT and His37(4-thiazolyl)Ala mutant construct were performed in DLPC bilayers using a previously described thiol–disulfide equilibrium method [28] where tetramer stability is determined by the relative amount of Cys19-mediated peptide dimer formation as a function of redox balance set by varying concentrations of glutathione and oxidized glutathione dimer in the experimental buffer. The presence of the C-terminal helix (residues ~50–62) in addition to the TM domain significantly enhances M2 tetramer stability (unpublished data), therefore shorter constructs and a relatively thin bilayer were used for this experiment so that some amount of dissociated protein was present to enable calculation of the equilibrium constant. Longer constructs such as M2(19–62) and/or thicker bilayers such as POPC result in virtually complete M2 tetramerization and thus cannot be used to determine dissociation constants.

Table 1
Thermodynamic stabilities of wild type and M2His37(4-thiazolyl)Ala mutant constructs. pK_{tet} is $-\log(K_{tet})$, where K_{tet} is the tetramer dissociation equilibrium constant.

Construct	pK_{tet} at pH 8
M2(19–46) wild type	8.4
M2(19–46) 4-thiazolylalanine	7.8

The results of thiol–disulfide equilibrium experiments on M2(19–46) WT and His37(4-thiazolyl)Ala mutant constructs in DLPC bilayers are shown in Table 1.

The data show that at pH 8 in bilayers, the wild-type and mutant constructs have roughly similar tetramer stabilities (within an order of magnitude), indicating that the introduction of the unnatural amino acid does not substantially destabilize the tetrameric assembly of the protein. This finding paves the way for functional experiments to assess the impact of the mutation on proton transport, activation, and inhibition.

3.2. M2(19–62) His37(4-thiazolyl)Ala is inactive at pH_{out} 7.4 but shows increasing amantadine sensitive activity at pH_{out} 4.9 and 2.4 comparable to activity of wild-type construct at pH 7.4 and 4.9 respectively

The results for M2(19–62) proteoliposomes in our semiquantitative flux assay (Fig. 2A) show that the construct forms a functional, amantadine-sensitive tetramer at bathing extraliposomal buffer pH values of 7.4 and 4.9. An initial transport rate of approximately 1 proton per second per tetramer is observed at pH_{out} 7.4, and increases to approximately 3 protons per second per tetramer at pH_{out} 4.9. The initial transport rate into WT peptide liposomes at pH_{out} 2.4 could not be calculated from the post-mixing flux curve because of very rapid liposome acidification during the 3 s sample mixing period and prior to data acquisition. Based on intraliposomal buffer pK_a and estimates of pre-mixing intraliposomal pH, it is estimated to be ~15–20 protons per second per tetramer during the mixing process. This rate is significantly lower than expected from other estimates of maximum M2 current in the literature [20–22,31], and may reflect dissociation or inactivation of the wild type protein at very acidic pH values [21,32]. Flux limitation by the amount of valinomycin used (~30 nM, active tetramer: valinomycin ~1:1) must also be considered but is less likely given the high (10^4) per second turnover rate of valinomycin [33] and saturating potassium concentrations. No inhibitory effect of amantadine on flux through the wild type construct was observed at bathing buffer pH of 2.4 (Fig. S2).

The M2(19–62) thiazolylalanine construct (Fig. 2B) was largely inactive at pH 7.4, as may be expected given the much lower pK_a of this sidechain as compared to histidine (in solution, ~2.55 vs 6.5 respectively). However, progressive proton flux activation was observed at pH 4.9 and especially pH 2.4, where significant proton currents (~1.5 per second per tetramer) were observed. At all pH values tested, the currents were almost fully amantadine sensitive, indicating a native-like conformation of the tetramer and its N-terminal aqueous pore where amantadine binds.

4. Discussion

The proton transport mechanism through M2 remains of interest not only for guiding design of new inhibitors of amantadine-resistant variants of the protein [13,34,35], but also from the perspective of a minimalistic model system for regulated, selective transmembrane charge transport and stabilization [1,18].

Since the initial postulation of two mechanistic hypotheses for M2 proton transport, the His37 electrostatic gate [8] and the His37 proton shuttle [10], the last several years have brought about an increasingly refined understanding of the structural and dynamic underpinnings that give rise to the functional complexity exhibited by M2. Overall, our understanding of M2 proton transport today [1,11,18,19,25] is remarkably consistent with the previously proposed proton shuttle mechanism [10] although it can now be interpreted within a wealth of atomic-level structural data increasingly derived in native-like lipid bilayers [18,19].

Our findings presented here further refine our mechanistic understanding of M2 proton transport by reinforcing its dependence on His37 side chain protonation and deprotonation as determined by its pK_a. In keeping with earlier results from chemical rescue experiments by Pinto et al. [27], we have been able to engineer a sterically similar yet electronically distinct His37 mutant variant with a markedly lower sidechain pK_a that preserves tetramer stability in bilayers but predictably shifts proton flux activation to a lower extraviral pH range where wild-type protein begins to lose some of its physiological properties such as amantadine sensitivity [21].

The unnatural 4-thiazole group, in addition to its steric resemblance of imidazole and lower pK_a, is, by contrast with imidazole, incapable of undergoing tautomerization. Our findings of native-like proton currents through the mutant construct at an appropriately lowered extraliposomal pH range indicate that proton transport through M2 can proceed independently of His37 tautomerization, presumably relying on side chain motion alone as suggested in recent ssNMR experiments [17–19].

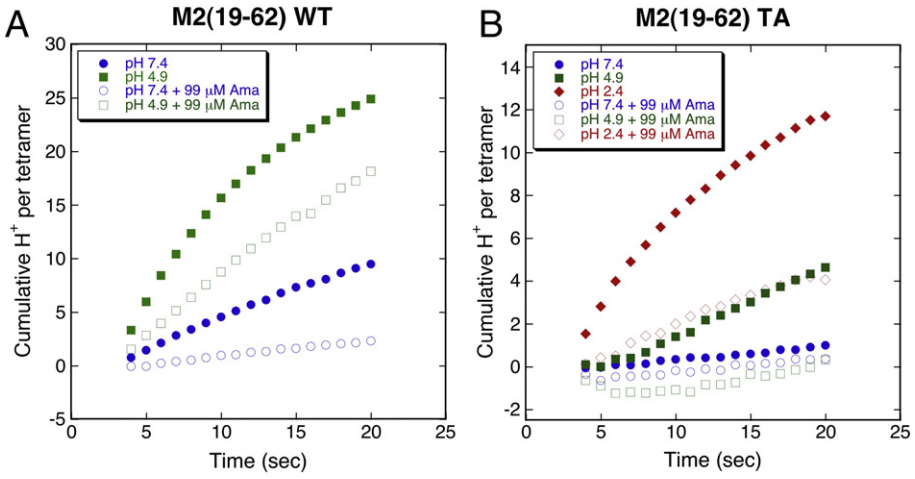

Fig. 2. Semiquantitative determination of inward proton flux through M2 19–62 proteoliposomes following control liposome flux subtraction at bathing buffer pH values as shown. Solid symbols, apo construct; outline symbols, with amantadine inhibition. A. Wild-type construct. B. ThiazolylAla mutant at position 37.

Finally, the 4-thiazolylAla mutant construct exhibits robust amantadine inhibition of currents at pH ranges where this construct is otherwise active and (at pH 2.4) where amantadine sensitivity by the wild-type protein begins to be lost, suggesting a similar, pH-tuned mode of inhibition amongst the two constructs and serving as an important internal control for demonstration of the specificity of the unnatural amino acid substitution.

In summary, our findings support the growing body of evidence that proton transport through M2 takes place predominantly via a pH-activated histidine shuttle mechanism. Specifically the mechanism is defined by the His37 side chain pK_a that may vary amongst an ensemble of transmembrane bundle conformations and as a function of tetrad protonation state for successive His37 sites. The kinetic cycle involves extraviral protonation of His37 imidazole by adjacent hydrogen bonded water molecules, and deprotonation on the extraviral aspect of the protein, with a side chain ring flip. Furthermore, at least for this close analog of His37, we can conclude that tautomer exchange is not required for the kinetic mechanism of conduction.

Disclosures

W.F.D. is on the scientific advisory board of InfluMedix and L.C. is employed by InfluMedix.

Acknowledgements

This research was funded by NIH grant GM56423 to W.F.D.

Appendix A. Supplementary data

Supplementary data to this article can be found online at http://dx.doi.org/10.1016/j.bbamem.2013.11.011.

References

[1] M. Hong, W. DeGrado, Structural basis for proton conduction and inhibition by the influenza M2 protein, Protein Sci. 21 (2012) 1620–1633.
[2] R. Bright, M. Medina, X. Xu, G. Perez-Oronoz, T. Wallis, X. Davis, L. Povinelli, N. Cox, A. Klimov, Incidence of adamantane resistance among influenza A (H3N2) viruses isolated worldwide from 1994 to 2005: a cause for concern, Lancet 366 (2005) 1175–1181.
[3] R. Bright, D. Shay, B. Shu, N. Cox, A. Klimov, Adamantane resistance among influenza A viruses isolated early during the 2005–2006 influenza season in the United States, JAMA 295 (2006) 891–894.
[4] C. Ma, A. Polishchuk, Y. Ohigashi, A. Stouffer, A. Schon, E. Magavern, X. Jing, J. Lear, E. Freire, R. Lamb, W. DeGrado, L. Pinto, Identification of the functional core of the influenza A virus A/M2 proton-selective ion channel, Proc. Natl. Acad. Sci. U. S. A. 106 (2009) 12283–12288.
[5] R. Acharya, V. Carnevale, G. Fiorin, B. Levine, A. Polishchuk, V. Balannik, I. Samish, R. Lamb, L. Pinto, W. DeGrado, M. Klein, Structure and mechanism of proton transport through the transmembrane tetrameric M2 protein bundle of the influenza A virus, Proc. Natl. Acad. Sci. U. S. A. 107 (2010) 15075–15080.
[6] C. Wang, R. Lamb, L. Pinto, Activation of the M2 ion channel of influenza virus: a role for the transmembrane domain histidine residue, Biophys. J. 69 (1995) 1363–1371.
[7] Y. Tang, F. Zaitseva, R. Lamb, L. Pinto, The gate of the influenza virus M2 proton channel is formed by a single tryptophan residue, J. Biol. Chem. 277 (2002) 39880–39886.
[8] M. Sansom, I. Kerr, G. Smith, H. Son, The influenza A virus M2 channel: a molecular modeling and simulation study, Virology 233 (1997) 163–173.
[9] I. Chizhmakov, F. Geraghty, D. Ogden, A. Hayhurst, M. Antoniou, A. Hay, Selective proton permeability and pH regulation of the influenza virus M2 channel expressed in mouse erythroleukaemia cells, J. Physiol. 494 (1996) 329–336.
[10] L. Pinto, G. Dieckmann, C. Gandhi, C. Papworth, J. Braman, M. Shaughnessy, J. Lear, R. Lamb, W. DeGrado, A functionally defined model for the M2 proton channel of influenza A virus suggests a mechanism for its ion selectivity, Proc. Natl. Acad. Sci. U. S. A. 94 (1997) 11301–11306.
[11] H. Zhou, A theory for the proton transport of the influenza virus M2 protein: extensive test against conductance data, Biophys. J. 100 (2011) 912–921.
[12] A. Polishchuk, J. Lear, C. Ma, R. Lamb, L. Pinto, W. DeGrado, A pH-dependent conformational ensemble mediates proton transport through the influenza A/M2 protein, Biochemistry 49 (2010) 10061–10071.
[13] J. Wang, Y. Wu, C. Ma, G. Fiorin, J. Wang, L. Pinto, R. Lamb, M. Klein, W. DeGrado, Structure and inhibition of the drug-resistant S31N mutant of the M2 ion channel of influenza A virus, Proc. Natl. Acad. Sci. U. S. A. 110 (2013) 1315–1320.
[14] A. Stouffer, R. Acharya, D. Salom, A. Levine, L. Di Constanzo, C. Soto, V. Tereshko, V. Nanda, S. Stayrook, W. DeGrado, Structural basis for the function and inhibition of an influenza virus proton channel, Nature 451 (2008) 596–599.
[15] J. Schnell, J. Chou, Structure and mechanism of the M2 proton channel of influenza A virus, Nature 451 (2008) 591–595.
[16] E. Khurana, M. Dal Peraro, R. DeVane, S. Vemparala, W. DeGrado, M. Klein, Molecular dynamics calculations suggest a conduction mechanism for the M2 proton channel from influenza A virus, Proc. Natl. Acad. Sci. U. S. A. 106 (2009) 1069–1074.
[17] F. Hu, K. Schmidt-Rohr, M. Hong, NMR detection of pH-dependent histidine–water proton exchange reveals the conduction mechanism of a transmembrane proton channel, J. Am. Chem. Soc. 134 (2012) 3703–3713.
[18] M. Sharma, M. Yi, H. Dong, H. Qin, E. Peterson, D. Busath, H. Zhou, T. Cross, Insight into the mechanism of the influenza A proton channel from a structure in a lipid bilayer, Science 330 (2010) 509–512.
[19] F. Hu, W. Luo, M. Hong, Mechanism of proton conduction and gating in influenza M2 proton channels from solid-state NMR, Science 330 (2010) 505–508.
[20] T. Leiding, J. Wang, J. Martinsson, W. DeGrado, S. Arskold, Proton and cation transport activity of the M2 proton channel from influenza A virus, Proc. Natl. Acad. Sci. U. S. A. 107 (2010) 15409–15414.
[21] E. Peterson, T. Ryser, S. Funk, D. Inouye, M. Sharma, H. Qin, T. Cross, D. Busath, Functional reconstitution of influenza A M2(22–62), Biochim. Biophys. Acta 1808 (2011) 516–521.
[22] T. Lin, C. Schroeder, Definitive assignment of proton selectivity and attoampere unitary current to the M2 ion channel protein of influenza A virus, J. Virol. 75 (2001) 3647–3656.
[23] J. Hu, R. Fu, K. Nishimura, L. Zhang, H.-X. Zhou, D. Busath, V. Vijayvergiya, T. Cross, Histidines, heart of the hydrogen ion channel from influenza A virus: toward an understanding of conductance and proton selectivity, Proc. Natl. Acad. Sci. U. S. A. 103 (2006) 6865–6870.
[24] H. Dong, M. Yi, T. Cross, H. Zhou, Ab initio calculations and validation of the pH-dependent structures of the His37–Trp41 quartet, the heart of acid activation and proton conductance in the M2 protein of Influenza A virus, Chem. Sci. 4 (2013) 2776–2787.
[25] M. Hong, K. Fritzsching, J. Williams, Hydrogen-bonding partner of the proton-conducting histidine in the influenza M2 proton channel revealed from 1H chemical shifts, J. Am. Chem. Soc. 134 (2012) 14753–14755.
[26] H. Dong, G. Fiorin, W. DeGrado, M. Klein, Exploring histidine conformations in the M2 channel lumen of the influenza A virus at neutral pH via molecular simulations, J. Phys. Chem. Lett. 4 (2013) 3067–3071.
[27] P. Venkataraman, R. Lamb, L. Pinto, Chemical rescue of histidine selectivity filter mutants of the M2 ion channel of influenza A virus, J. Biol. Chem. 280 (2005) 21463–21472.
[28] L. Cristian, J. Lear, W. DeGrado, Use of thiol–disulfide equilibria to measure the energetics of assembly of transmembrane helices in phospholipid bilayers, Proc. Natl. Acad. Sci. U. S. A. 100 (2003) 14772–14777.
[29] L. Cristian, J. Lear, W. DeGrado, Determination of membrane protein stability via thermodynamic coupling of folding to thiol–disulfide interchange, Protein Sci. 12 (2003) 1732–1740.
[30] N. Dencher, P. Burghaus, S. Grzesiek, Determination of the net proton-hydroxide ion permeability across vesicular lipid bilayers and membrane proteins by optical probes, Methods Enzymol. 127 (1986) 746–760.
[31] J. Mould, H.-C. Li, C. Dudlack, J. Lear, A. Pekosz, R. Lamb, L. Pinto, Mechanism for proton conduction of the M2 ion channel of influenza A virus, J. Biol. Chem. 275 (2000) 8592–8599.
[32] D. Salom, B. Hill, J. Lear, W. DeGrado, pH-dependent tetramerization and amantadine binding of the transmembrane helix of M2 from the influenza A virus, Biochemistry 39 (2000) 14160–14170.
[33] T. Franklin, G. Snow, Biochemistry and molecular biology of antimicrobial drug action, Springer, New York, 2005. 56.
[34] X. Zhao, Y. Jie, M. Rosenberg, J. Wan, S. Zeng, W. Cui, Y. Xiao, Z. Li, Z. Tu, M. Casarotto, W. Hu, Design and synthesis of pinanamine derivatives as anti-influenza A M2 ion channel inhibitors, Antiviral Res. 96 (2012) 91–99.
[35] E. Torres, M. Duque, E. Vanderlinden, C. Ma, L. Pinto, P. Camps, M. Froeyen, S. Vazquez, L. Naesens, Role of the viral hemagglutinin in the anti-influenza virus activity of newly synthesized polycyclic amine compounds, Antiviral Res. 99 (2013) 281–291.